PERGAMON

International Journal of Heat and Mass Transfer 44 (2001) 1963–1972

International Journal of HEAT and MASS TRANSFER

www.elsevier.com/locate/ijhmt

Stability of supercritical fluid flow in a single-channel natural-convection loop

Vijay Chatoorgoon [1]

Atomic Energy of Canada Ltd, Chalk River Laboratories, Chalk River, Ontario, Canada K0J 1J0

Received 24 September 1999; received in revised form 19 June 2000

Abstract

In this paper, supercritical flow stability in a single-channel, natural-convection loop is examined using a non-linear numerical code. A theoretical stability criterion is also developed to verify the numerical prediction. Good agreement between the numerical and analytical results was obtained. The mode of instability identified is purported to be different from the traditional instabilities associated with two-phase flow. The understanding derived is discussed. © 2001 Elsevier Science Ltd. All rights reserved.

1. Introduction

CANDU-X [1] is one of the advanced reactor concepts presently being assessed at AECL. This new generation of reactor will contain more inherent safety features and is expected to significantly reduce unit energy cost. The primary coolant presently being considered is light water and the pressure, designed to be at 25 MPa, is in the supercritical range. The higher core coolant temperature is aimed at improving thermodynamic efficiency. Both forced and natural-convection modes for the primary circuit are under consideration.

Flow instability at subcritical flow conditions has received considerable, in-depth study by many investigators. Flow instability at supercritical conditions, however, has not been investigated to a similar degree, likely because existing nuclear reactors and most fossil power stations operate at subcritical flow conditions.

An important safety feature being considered in this design is the removal of the core heat through natural circulation. Thus, stable natural-convection flow is a design pre-requisite. Flow instability, if it does occur in supercritical fluid flow, must be accurately predicted and circumvented through effective, defensible means. The first phase of this study, therefore, is an investigation of the supercritical flow stability of a single-channel, natural-circulation loop.

The findings described here were obtained from simulations with a non-linear numerical stability code. An analytical model of supercritical flow instability in an idealized single-channel, natural-convection configuration is also developed and the understanding derived is discussed.

2. Problem definition

To help define the problem, a simple, single-channel, natural-convection configuration was chosen for study. It is described as follows.

The configuration is a constant area loop, shown in Fig. 1 with dimensions. It is essentially a closed system, with sides BC and DA vertical and sides AB and CD horizontal. The boundary conditions are as follows: the inlet and outlet pressures are constant and equal, and the inlet temperature is constant. These boundary conditions can be achieved in practice by connecting the inlet and outlet to a pressurizer, or to a surge tank. The pressurizer will therefore comprise another degree of freedom.

[1] Present address: Department of Mechanical Engineering, University of Manitoba, 15 Gillson St., Winnziey, Manitoba, Canada R3T 5V6.

E-mail address: chatoorv@mad.scientist.com (V. Chatoorgoon).

PII: S0017-9310(00)00218-0

Nomenclature

A	flow area (m^2)
D	hydraulic diameter (m)
f	friction factor
G	mass flux ($kg/m^2/s$)
G_m	maximum mass flux ($kg/m^2/s$)
g	gravitation constant (m/s^2)
h	fluid enthalpy (kJ/kg)
h_1	cold-side enthalpy (kJ/kg)
h_2	hot-side enthalpy (kJ/kg)
h_{2_b}	hot-side enthalpy at the maximum mass flux (kJ/kg)
h_t	height of loop (m)
p	static pressure (N/m^2)
Q	total channel power (kW)
Q_b	power at the maximum mass flux (kW)
z	axial distance (m)

Non-dimensional variables

G^*	non-dimensional mass flux
G^*_m	non-dimensional maximum mass flux
Q^*_b	non-dimensional bounding power
R^*	non-dimensional density

Greek symbols

ρ	fluid density (kg/m^3)
ρ_1	cold-side density upstream of heater (kg/m^3)
ρ_2	hot-side density (kg/m^3)
ρ_3	fluid density downstream of heat sink (kg/m^3)
ρ_{2_b}	hot-side density at the maximum mass flux (kg/m^3)
β	inclination to the horizontal (degree)
θ	$f_2 z_2/(f_1 z_1 + f_3 z_3)$
ξ	$\sqrt{2gDh_t}/f_2 z_2$ (m/s)
Φ	$-\theta + \sqrt{\theta^2 + \theta}$

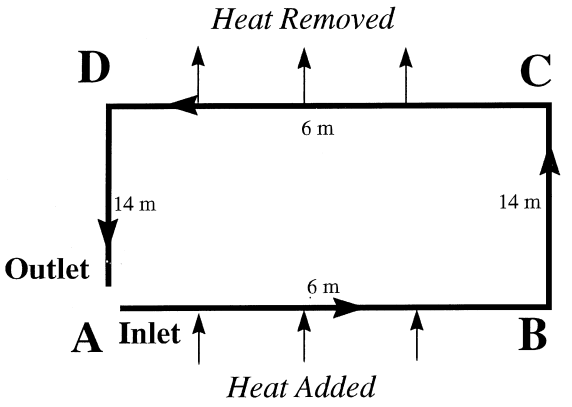

Area	=	0.0044 m^2
D	=	0.0785 m
f_1	=	0.167
f_2	=	0.0567
f_3	=	0.0381
z_1	=	3.0 m
z_2	=	20.0 m
z_3	=	17.0 m

Fig. 1. Schematic of loop.

An inlet pressure of 25 MPa and an inlet temperature of 350°C were imposed. A distributed heat source was applied along the lower horizontal leg AB and a distributed heat sink was applied along the upper horizontal leg CD. Friction factors are given in Fig. 1, and they were the effective net friction factor that also includes the obstruction loss coefficient. A constant and axially uniform heat flux was assumed. Hence any temperature dependency on the wall-film thermal conductivity is ignored.

This system was analyzed first with the SPORTS [2] thermalhydraulic stability code. The derived steady-state solution of this natural-convection system is shown in Fig. 2(a). The flow rate initially increases with power, attains a maximum at about 3.8 MW, and then decreases with power. It is usual for a natural-convection-driven flow to increase with power, but the decrease in flow rate with increasing power was a surprising result. Such an occurrence had not previously been obtained from numerical calculations of subcritical (two-phase) flows.

Some SPORTS stability simulations of these steady-state solutions were also performed. The results are shown in Fig. 2(b) for three different powers: 4.0, 4.5 and 5.0 MW. The 4.0 MW response, which is close to the peak of the steady-state profile in Fig. 2(a), is stable, while the 4.5 and 5.0 MW responses are unstable, with the 5.0 MW being more unstable than the 4.5 MW response.

The positive slope of the flow-power characteristic comprises the stable solutions, while the negative slope comprises the unstable solutions. The power corresponding to the maximum flow rate, of the flow-power characteristic, therefore approximately defines the bounding power, Q_b, for stable operation.

3. The SPORTS code

The SPORTS non-linear code [2] was originally developed to investigate the stability of flows at low pressure due to subcooled boiling, and to perform transient simulations of thermalhydraulic and neutron-kinetic coupled dynamics. As the general 1-D conservation equations are solved using a fully implicit

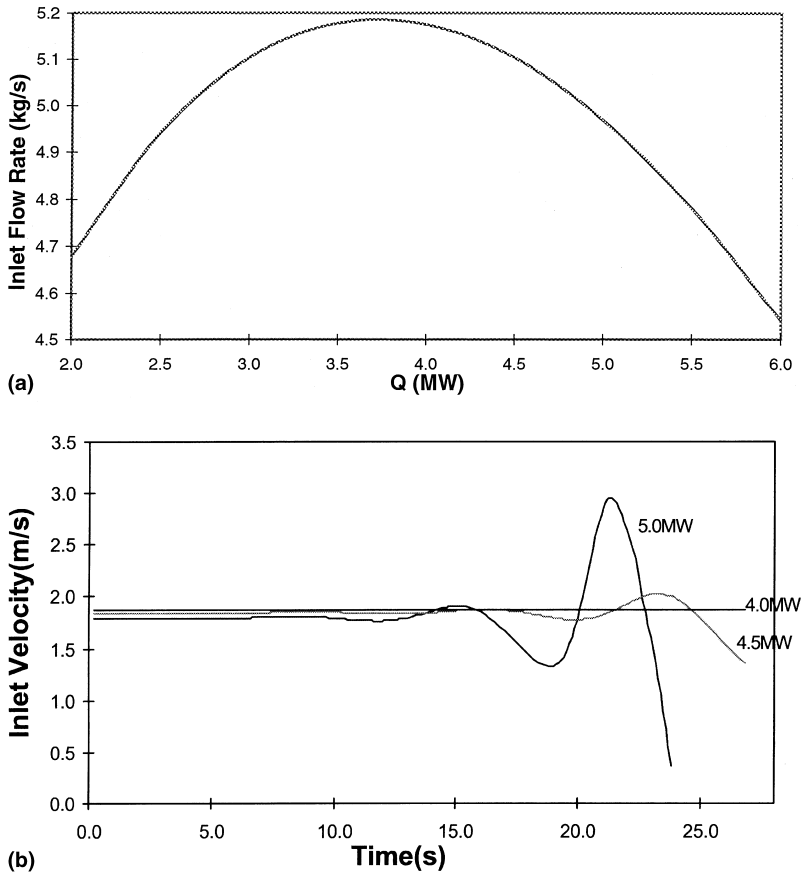

Fig. 2. (a) Steady-state solution of loop (Fig. 1) with distributed source and sink. (b) SPORTS stability simulation of loop (Fig. 1) with distributed source and sink.

numerical algorithm, the code was deemed suitable for modeling supercritical flow stability providing the built-in algorithms remained numerically sound and convergent for the supercritical properties. SPORTS numerical algorithms circumvented the use of property derivatives. This may be of advantage in computations near the critical point, where some fluid properties vary considerably with temperature.

The SPORTS code determines flow instability by introducing a perturbation in the inlet flow rate and executing a real-time transient. If the system is stable, the perturbation will diminish with time and vanish, restoring the original steady-state solution. If the system is unstable, the perturbation will grow, precipitating flow oscillations, or a flow excursion, and the initial steady state will not be recovered.

The SPORTS code has been formerly sufficiently benchmarked against two-phase instability experiments [3,4] and natural-circulation flows. However, it has not been benchmarked against supercritical-flow instability experiments. The STEAM [5] property package, which is valid in the supercritical range, was implemented into the SPORTS code for the simulations presented here.

4. Analytical model of flow instability

To develop an analytical model of the observed phenomenon, the simple configuration defined in Fig. 1 is considered, but with the following modification: the heat source and sink, instead of being uniformly distributed along sides AB and CD, were assumed to be point sources situated at the middle of sides AB and CD. This helped to simplify the analysis and facilitates a better understanding of the underlying physics. For an axially uniform heat flux, the enthalpy distribution along the heated length would be linear, while the temperature distribution, and hence also the density distribution, would be highly non-linear due to their characteristics across the critical temperature. This would pose a problem in the spatial integration of the density terms (of the momentum equation) in an analytical derivation.

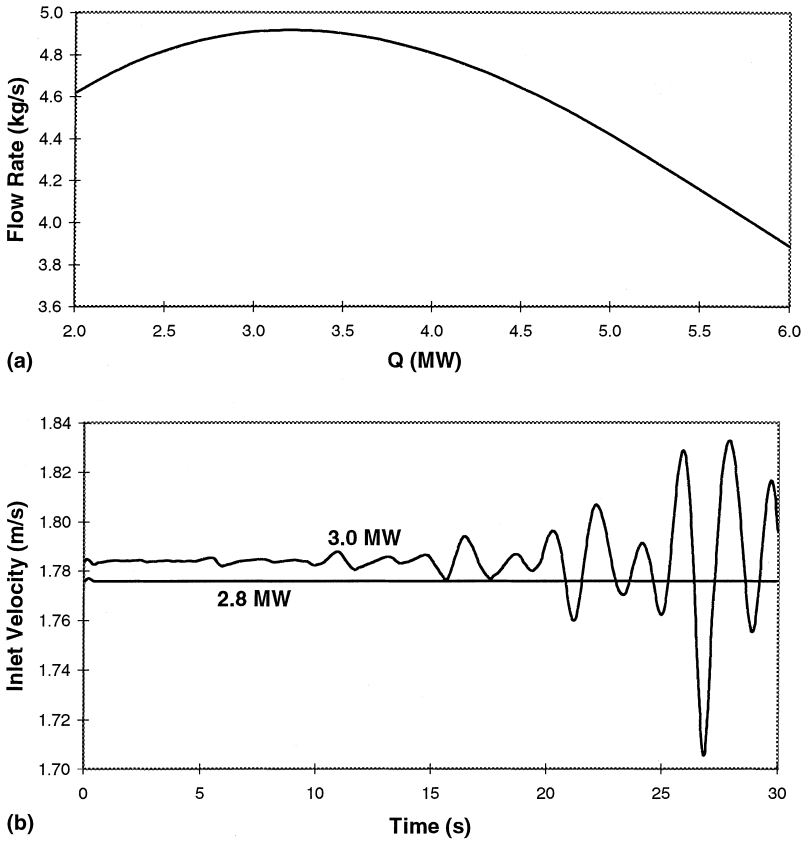

Fig. 3. (a) Steady-state solution of loop (Fig. 1) with point source and sink. (b) SPORTS stability simulation of loop (Fig. 1) with point source and sink.

This problem was circumvented by assuming point sources for the heat source and heat sink.

The corresponding SPORTS steady-state solution for this configuration is shown in Fig. 3(a) and the stability simulation is shown in Fig. 3(b). The steady-state flow versus power characteristic, for a point heat source and sink is qualitatively similar to that of a distributed heat source and sink (Fig. 2), except that the peak flow rate in Fig. 4 now occurs at a power of about 3.2 MW, instead of at 3.8 MW. In other words, the point heat source and sink approximation merely reduces the power at which the maximum flow rate occurs.

The works of Whittle and Forgan [6], Duffey and Hughes [7,8] and Rohatgi and Duffey [9] have shown that the instability boundary of two-phase (subcritical) flow can be analytically approximated by solving the system steady-state equations for the minimum zero slope of the Δp-flow characteristic (i.e., where Δp attains a minimum with the flow rate), and using this solution to obtain the flow conditions at the instability boundary.

A comparison of the Duffey and Hughes [8] analytical model against various data sets yielded good agreement. This confirmed that the minimum zero slope of the Δp-flow characteristic is a *bonafide* approximation for the stability boundary of two-phase flow. Any differences between theory and experiment were attributed to the omission of non-equilibrium effects in the Duffey and Hughes model. For the traditional two-phase flow

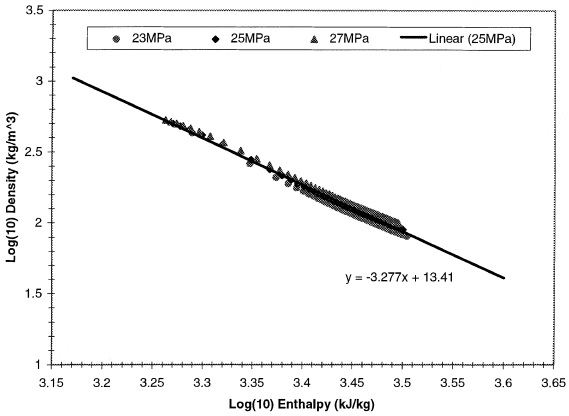

Fig. 4. Density versus enthalpy ($T = 376$–$500°C$).

(subcritical) situation, the system is unstable on the negative slope of the Δp-flow characteristic.

For supercritical fluid flow in natural-convection, single-channel systems, Δp from the system inlet to outlet is fixed, and hence constant, for all steady-state flow rates. Hence, the minimum zero slope of the Δp-flow characteristic is meaningless for this configuration, and a different criterion is required to derive the instability boundary from the system steady-state characteristics.

It is hereby postulated that the instability boundary for a single-channel, natural-circulation loop at supercritical conditions can be approximated by the criterion

$$\frac{\partial(\text{flow})}{\partial(Q)} = 0, \tag{1}$$

where Q is the channel power. I emphasize here that, from a strict mathematical sense, Eq. (1) is an *approximation* used to obtain the stability boundary, and is not an exact criterion. The accuracy of this approximation is not known, but from an engineering perspective, this approximation may be acceptable and useful for obtaining an analytical solution by which insights can be gleaned.

Dispensing with the usual practice of proving that this occurs at a maximum, and not a minimum, since the steady-state characteristic (Fig. 2(a)) shows that the zero slope occurs only at a maximum, the constant area loop (Fig. 1) with point heat source and sink is now considered. The steady-state continuity equation gives

$$\text{Mass flux, } G = \text{constant}. \tag{2}$$

The momentum equation for steady state is

$$\frac{\partial}{\partial z}(G^2/\rho) = -\frac{\partial p}{\partial z} + \rho g \sin\beta - \frac{f}{2D}(G^2/\rho),$$

where $\beta = 0$ for horizontal flow, 90° for downflow and −90° for upflow. As before, f is the net effective friction factor, which includes the obstruction loss coefficient. Integrating the momentum equation around the closed loop

$$\oint \rho g \sin\beta \, \mathrm{d}z = \oint \frac{f}{2D}\left(\frac{G^2}{\rho}\right) \mathrm{d}z.$$

Assuming that the heat source and sink are of equal magnitude, ρ_1 is the unheated (cold) density, ρ_2 the heated (hot) density, z_1 the cold length from the loop entrance to the heat source, f_1 the corresponding friction factor, z_2 the hot length between the heat source and sink, f_2 the corresponding friction factor, z_3 the cold length downstream of the heat sink to the end of the loop and f_3 is the corresponding friction factor. Then

$$g(\rho_1 - \rho_2)h_t = \frac{G^2}{2D}\left(\frac{f_1 z_1 + f_3 z_3}{\rho_1} + \frac{f_2 z_2}{\rho_2}\right),$$

or

$$G^2 = \frac{2Dgh_t(\rho_1 - \rho_2)}{\{((f_1 z_1 + f_3 z_3)/\rho_1) + (f_2 z_2/\rho_2)\}}. \tag{3}$$

The energy equation gives

$$Q = GA(h_2 - h_1) \tag{4}$$

and the equation of state is assuming that there is no significant pressure dependence

$$\rho_2 = f(h_2). \tag{5}$$

Differentiating Eq. (3) with respect to ρ_2 and ignoring the dependency of the friction factor on ρ_2 and temperature gives

$$\frac{\partial G}{\partial \rho_2} = G\left[\frac{f_2 z_2 (G/\rho_2)^2 - 2gDh_t}{4gDh_t(\rho_1 - \rho_2)}\right]. \tag{6}$$

Differentiating Eq. (4) with respect to G

$$\frac{\partial Q}{\partial G} = A(h_2 - h_1) + GA\frac{\partial h_2}{\partial G} = \frac{Q}{G} + GA\left(\frac{\partial h_2}{\partial \rho_2}\right)\Big/\left(\frac{\partial G}{\partial \rho_2}\right). \tag{7}$$

Combining Eqs. (6) and (7) and simplifying gives

$$\frac{\partial G}{\partial Q} = \frac{f_2 z_2 (G/\rho_2)^2 - 2gDh_t}{(Q/G)\{f_2 z_2 (G/\rho_2)^2 - 2gDh_t\} + 4A(\partial h_2/\partial \rho_2)gDh_t(\rho_1 - \rho_2)}. \tag{8}$$

In Eq. (8), $\partial G/\partial Q = 0$, when

$$\left(\frac{G_\mathrm{m}}{\rho_{2_\mathrm{b}}}\right)^2 = \frac{2gDh_t}{f_2 z_2} = \xi^2,$$

or

$$G_\mathrm{m} = \rho_{2_\mathrm{b}}\xi, \quad \text{where } \xi^2 \equiv \frac{2gDh_t}{f_2 z_2}, \tag{9}$$

where G_m is the maximum value of the mass flux for a given geometry and ρ_{2_b} is the corresponding hot-side density at that mass flux. To derive the corresponding power at the stability boundary, Q_b, the following simplified state relation is introduced for the hot side:

$$\rho_2 = \frac{B}{h_2^{\eta_2}}. \tag{10}$$

The constants B and η_2 can be deduced by plotting h_2 versus ρ_2 on log–log plots and determining the slope (this gives η_2) and ordinate intersection (this gives B). Of course, B and η_2 may vary with pressure and temperature range, but the above form is a realistic representation that has proven to be useful for this

analysis. Fig. 4 plots ρ_2 versus h_2 at 25 MPa and for the temperature range 376–500°C. To a very good approximation, $\log\rho$ versus $\log h$ is linear in the temperature range of interest. Fig. 4 yields $B = 1.7418 \times 10^{23}$ and $\eta_2 = 3.277$.

From the energy equation (4)

$$Q_b = G_m A(h_{2_b} - h_1). \tag{11}$$

Using Eq. (10)

$$Q_b = G_m A\left(\left(\frac{B}{\rho_{2_b}}\right)^{1/\eta_2} - h_1\right). \tag{12}$$

Eq. (3) becomes, at the stability boundary

$$\left(\frac{G_m}{\xi}\right)^2 = \frac{(\rho_1 - G_m/\xi)}{(1/\theta\rho_1) + (\xi/G_m)}, \tag{13}$$

where

$$\theta \equiv \frac{f_2 z_2}{f_1 z_1 + f_3 z_3}. \tag{14}$$

Rearranging Eq. (13) gives

$$\left(\frac{1}{\theta\rho_1}\right)\left(\frac{G_m}{\xi}\right)^2 + 2\left(\frac{G_m}{\xi}\right) - \rho_1 = 0, \tag{15}$$

which is a quadratic equation with two roots. Solving Eq. (15) for the two roots gives

$$\left(\frac{G_m}{\xi}\right) = \left\{-\theta \pm \sqrt{\theta^2 + \theta}\right\}\rho_1. \tag{16}$$

Of the two roots, only the one corresponding to a positive (G_m/ξ) is relevant; hence

$$\left(\frac{G_m}{\xi}\right) = \rho_1 \Phi, \tag{17}$$

where

$$\Phi \equiv -\theta + \sqrt{\theta^2 + \theta}, \tag{18}$$

$$\therefore G_m = \xi\rho_{2_b} = \xi\rho_1\Phi, \quad \therefore \rho_{2_b} = \rho_1\Phi \tag{19a}$$

and

$$h_{2_b} = \left(\frac{B}{\rho_1\Phi}\right)^{1/\eta_2}. \tag{19b}$$

Substituting Eqs. (17) and (19a) into Eq. (12) gives

$$Q_b = A\rho_1\xi\Phi\left[\left(\frac{B}{\rho_1\Phi}\right)^{1/\eta_2} - h_1\right]. \tag{20}$$

Eq. (20) defines the approximate power at the stability boundary, Q_b, as a function of inlet conditions and loop geometry for a single-channel, natural-circulation system with supercritical flow. Note that Eq. (20) no longer contains the flow rate or hot-side conditions. This is expected, since the power uniquely defines the flow rate and outlet conditions of a natural-circulation system with given geometric characteristics. While Eq. (20) was developed for a point heat source and sink, it is believed that the trends described would apply equally for a distributed heat source and sink.

4.1. Normalizing

For convenience, the additional non-dimensional parameters G, G_m^*, Q_b^* and R^* are introduced, where

$$G^* \equiv \frac{G}{\rho_1\xi}, \tag{21}$$

$$G_m^* \equiv \frac{G_m}{\rho_1\xi}, \tag{22}$$

$$Q_b^* \equiv \frac{Q_b}{AG_m h_1} \equiv \frac{Q_b}{A\rho_1 h_1 \xi G_m^*}, \tag{23}$$

$$R^* \equiv \rho_2/\rho_1. \tag{24}$$

Thus, the following identities are obtained:

$$G^{*2} = \frac{(1 - R^*)}{(1/\theta + 1/R^*)}, \tag{25}$$

$$G_m^* = \Phi = -\theta + \sqrt{\theta^2 + \theta}, \tag{26}$$

$$Q_b^* = \left(\frac{B^*}{\Phi}\right)^{1/\eta_2} - 1, \quad \text{where } B^* = \frac{B}{\rho_1 h_1^{\eta_2}} \tag{27}$$

and

$$R_b^* = \Phi \ (= G_m^*). \tag{28}$$

The non-dimensional parameters, Eqs. (21)–(28), may be useful for scaling purposes and experimental design.

5. Solution of analytic equations

The analytic equations derived above, for the stability boundary of supercritical fluid flow in a single-channel, natural-convection loop containing a point heat source and sink, assumed that the source and sink strengths were equal in magnitude. Solutions are presented for some of the derived analytical expressions to facilitate an understanding of the parametric trends. For the supercritical cases presented, the inlet temperature was usually 350°C (unless otherwise stated) and the inlet pressure was 25 MPa.

When the stability condition, Eq. (9), is satisfied, Eq. (6) also yields $\partial G/\partial\rho_2 = 0$. This means that the maximum flow rate, on the flow-ρ_2 characteristic, also

coincides with the maximum flow rate on the flow-power characteristic. Power affects ρ_2, which in turn affects the flow rate, so this result is not entirely surprising.

Consequently, some insight into the predictions of Eq. (3), which defines the steady flow rate around the loop, can be gleaned. Decreasing ρ_2, from low power, say, increases the flow rate initially because of the increasing numerator term $(\rho_1 - \rho_2)$ – the gravity-driven term. However, as ρ_2 continues to decrease with increasing power, the increasing frictional term in the denominator, $(f_2 z_2)/\rho_2$, dominates at some point, and the loop mass-flow rate begins to decrease after attaining a maximum. This occurs at supercritical conditions because of the large thermal expansion rate (rate of change of specific volume with enthalpy) across the critical point.

The stability relation, Eq. (9), is really a balance between the gravitational 'lift' force and the frictional 'drag' force, similar to that discussed by Duffey and Hughes [8] for two-phase flow.

Fig. 5 shows the solution of Eq. (27) for the non-dimensional 'bounding' power, Q_b^*, and the non-dimensional friction parameter, θ, plotted versus Φ, R^* or G^* for an inlet temperature of 350°C and an inlet pressure of 25 MPa. As stated previously, the maximum possible value of Φ, R^* or G^* is 0.5. In the region labeled 'UNSTABLE', in Fig. 5, the slope of the 'flow versus power' characteristic is negative and the system will be dynamically unstable. In the region labeled 'STABLE', the reverse holds true and the system will be stable.

Figs. 6(a) and (b) depict a similar result, plotted on different scales for more clarity. Q_b^* versus θ is plotted to show that the non-dimensional bounding power, Q_b^*, decreases monotonically with θ. Fig. 6(a) and (b) also show that Φ, R^* or G^* increases monotonically with θ to a maximum value of 0.5.

Fig. 7 shows the effect on bounding power of variations in either f_1, or f_2, or f_3 (one friction factor was varied while the other two were held constant). The effect of reducing f_2 always increases the bounding power. However, the effect of reducing f_1, or f_3, may increase or decrease the bounding power, since the bounding power first increases to a maximum with decreasing friction factor and then decreases with further decreases in that friction factor.

The analytical relations derived also indicate that, on the flow-power characteristic, there is only one maximum and no true minimum. Numerical results at increasingly higher powers confirmed this finding (results not shown). As the power was increased beyond Q_b, for a fixed inlet temperature, the flow rate decreased, and then leveled off to almost a constant value with increasing power.

5.1. Parameters affecting stability

Eq. (20) gives some useful insight into the parameters that affect Q_b, the power at the instability boundary.

Lower inlet temperature. Eq. (20) predicts that decreasing the inlet temperature would cause a significant increase of Q_b. Figs. 8(a) and (b) show the effect of inlet temperature on the bounding power, Q_b. The bounding power goes up significantly with lower inlet temperatures.

Flow area. Increasing the flow area, A, and hydraulic diameter, D, (the latter increases ξ) would cause an increase in Q_b. In addition, f_2 would be lowered, which would contribute to a further increase in ξ and, hence, bounding power.

Friction. A reduction in the hot-side friction factor, f_2, would always result in an increase in the bounding power, similar to two-phase flow instability. However, an increase in the cold-side friction-factor, f_1 or f_3, would not necessarily lead to an increase in the bounding power, as would be the case for two-phase flow instability. Fig. 7 shows that there could be a decrease in the bounding power.

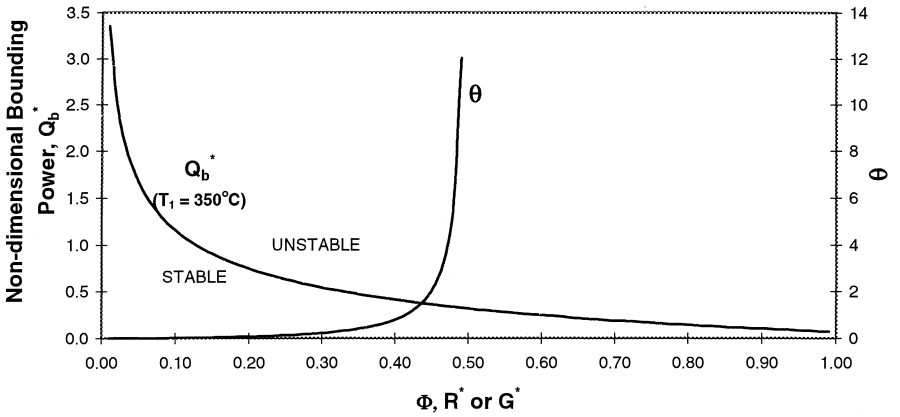

Fig. 5. Parameters at stability boundary for $p = 25$ MPa.

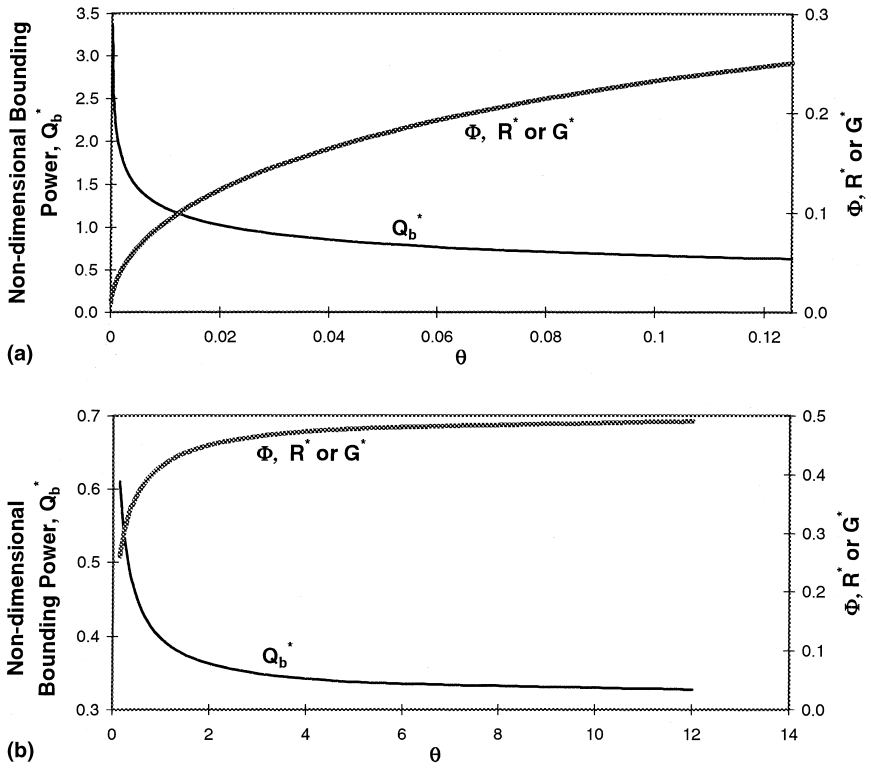

Fig. 6. (a) Parameters at stability boundary for $p = 25$ MPa. (b) Parameters at stability boundary for $p = 25$ MPa.

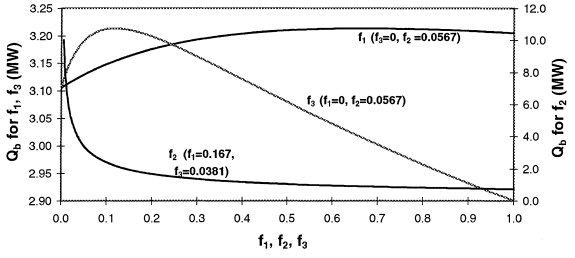

Fig. 7. Effect of friction factors on bounding power.

6. Verification of analytical equations

The configuration for which the preceding analytical expressions were derived (Fig. 1, but with a point heat source at the middle of AB and a heat sink in the middle of CD) was also simulated using the SPORTS code, to verify the predictions of the derived analytical relations. The friction factors were $f_1 = 0.167$, $f_2 = 0.0567$ and $f_3 = 0.0381$. The hydraulic diameter was 0.0785 m, the flow area was 0.0044 m^2, z_1 was 3.05 m, z_2 was 20.1 m and z_3 was 17.05 m. The vertical height of the loop, h_t, was 14 m.

The SPORTS results, given in Fig. 3(b), shows the responses for 2.8 and 3.0 MW. The 2.8 MW response is clearly stable, while the 3.0 MW response is just unstable, noting the very sensitive scale used on the ordinate. The conclusion from this simulation is that 3.0 MW is just about the stability boundary, according to SPORTS. Solving the analytical relation, Eq. (20), the bounding power, Q_b, was calculated to be 3.19 MW, approximately 6% higher than the SPORTS stability prediction.

This is considered to be good agreement, because of the following two reasons: (1) the SPORTS model approximated the point heat source and sink with a single node of length 0.1 m, rather than a node of zero length used in the analytical model, and (2) the analytical relations derived above for the stability boundary are only approximate expressions. Therefore, some discrepancy between the code prediction and the analytical solution was expected.

The period of oscillation of the 3.0 MW case was about 2.0 s. The loop transit time was about 22 s, approximately 10 times the period of oscillation. This is significantly different from the period of 6.4 s in Fig. 2 for the same loop, except that the heat source and sink are distributed along 6.1 m and are not point sources. It seems that the length of the heated section is an important parameter for defining the period of oscillation.

Other parameters were also tested to assess their effect on the stability boundary, as predicted by the derived relations. For example, the friction factors (f_1, f_2, f_3)

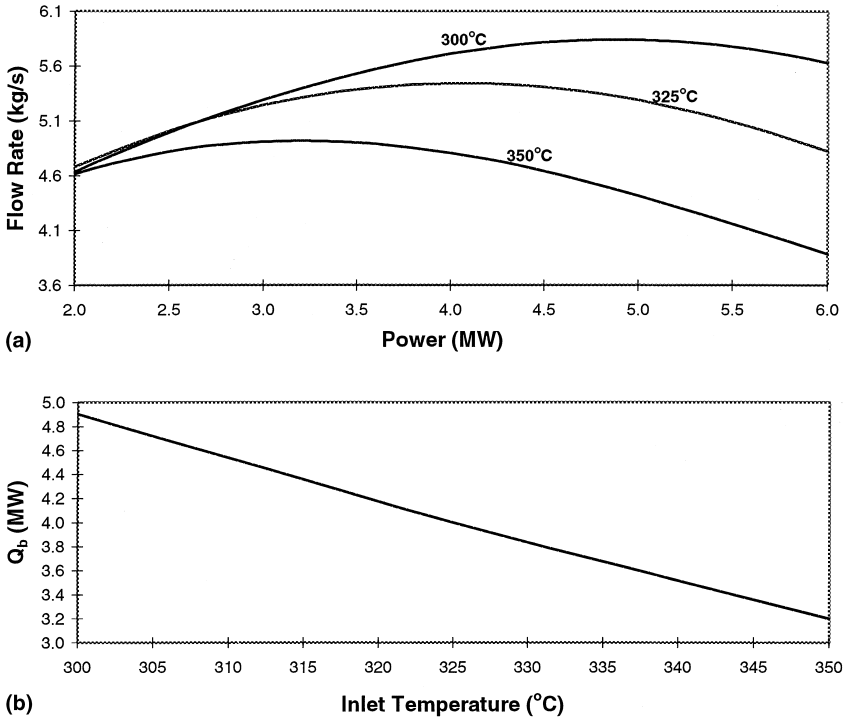

Fig. 8. (a) Steady-state solution with point sources at different inlet temperatures. (b) Effect of inlet temperature on bounding power.

were altered to maintain a constant θ while doubling f_2. Eq. (21) predicted that Q_b would be *reduced* by $\sqrt{2}$. SPORTS stability simulations confirmed this trend.

7. Discussion

The good agreement between the numerical and analytical solutions on the power at the maximum flow rate rules out any possibility of a numerical artifact being the cause of the decreasing flow rate with increasing power. Further, assessment showed that the SPORTS' numerical procedure converged well at every node and that the iteration on the inlet mass-flow rate always converged properly. Spatial convergence was demonstrated by increasing the number of nodes until closely similar solutions were obtained.

On the positive slope of the flow-power (or the negative slope of the flow-ρ_2) characteristic, a positive flow perturbation at a fixed power would result in an increase in outlet (heated) density, which would tend to reduce the initial flow perturbation and restore the loop's original flow rate.

On the negative slope of the flow-power (or the positive slope of the flow-ρ_2) characteristic, a positive flow perturbation at a fixed power would result in an increase in outlet (heated) density, which would tend to amplify the perturbation in the flow rate. Thus, the ensuing response would be a divergent one.

The point heat source and sink approximation is actually conservative, as it yields a lower bounding power than a distributed heat source and sink. In practice, it would be more accurate to generate the steady-state flow-power characteristic from a numerical code. It would also be advisable to include the effect of temperature on the friction factor. This effect was ignored in this study.

8. Conclusions and recommendations

A new type of flow instability has been obtained numerically and analytically for supercritical fluid flow in single-channel, natural-circulation loops. To the author's knowledge, this type of instability has not been reported before.

An idealized analytical model of the instability was developed, which confirmed the numerical predictions. It is recommended that experiments be conducted to confirm, or deny, this finding. It is also recommended that analyses be performed that includes a variation of the wall-film heat-transfer coefficient with temperature.

Non-dimensional parameters were derived that would be useful for scaling purposes, or correlating data. In

general, it would be desirable to always operate on the positive slope of the flow-power (or negative slope of the flow-ρ_2) characteristic.

Acknowledgements

Sincere thanks are expressed to Dr. R. Duffey, Dr. M. Carver and Dr. H. Rummens for review of the manuscript and helpful discussions.

References

[1] G.R. Dimmick, N.J. Spinks, R. Duffey, An advanced CANDU reactor with supercritical water coolant: conceptual design features, in: Proceedings of the Pacific Basin Nuclear Conference, 4–8 May 1998.

[2] V. Chatoorgoon, A simple thermalhydraulic stability code, Nucl. Eng. Design 93 (1986) 51–67.

[3] G.R. Dimmick, V. Chatoorgoon, Experimental and analytic investigation of two-phase stability in a natural circulation loop, ASME 85-WA/HT-16, ASME Winter Meeting, November 1985.

[4] V. Chatoorgoon, G.R. Dimmick, M.B. Carver, Modelling of low pressure subcooled boiling instability experiments, Instability in Two-Phase Systems, ASME Winter Meeting, 1993.

[5] A.H. Harvey, A.P. Peskin and S.A. Klein, NIST/ASME Steam Properties, version 2.1, US Department Of Commerce, Technology Administration, National Institute of Standards and Technology, December 1997.

[6] R.H. Whittle, R. Forgan, A correlation for the minima in the pressure drop versus flow-rate curves for subcooled water flowing in narrow heated channels, Nucl. Eng. Design 6 (1967) 89–99.

[7] R.B. Duffey, E.D. Hughes, Static flow instability onset in tubes, channels, annuli and rod bundles, in: Proceedings of the ASME, Heat Transfer Division, Thermal Hydraulics of Advanced Nuclear Reactors, 150, 1990, pp. 145–159.

[8] R.B. Duffey, E.D. Hughes, Static flow instability onset in tubes, channels, annuli and rod bundles, Int. J. Heat Mass Transfer 34 (10) (1991) 2483–2496.

[9] U.S. Rohatgi, R.B. Duffey, Natural circulation and stability limits in advanced plants: the Galilean law, in: Proceedings of the International Conference on New Trends in Nuclear System Thermohydraulics, Primary and Secondary Thermohydraulics, vol. 1, Pisa, Italy, 30 May 1994–2 June, pp. 177–185.